nature communications

Article

https://doi.org/10.1038/s41467-026-73612-0

Permafrost carbon release scales linearly with overshoot warming mediated by AMOC tipping

Received: 9 July 2025

Accepted: 14 May 2026

Published online: 16 July 2026

Check for updates

Norman Julius Steinert[1,2] ✉, Jörg Schwinger[2], Eleanor Burke[3], Biqing Zhu[4], Thomas Gasser[4], Gregory Munday[3,5], Camilla Mathison[3,6], So-Won Park[7] & Hanna Lee[8]

Overshooting global warming targets risks irreversible Earth system changes. However, uncertainties remain in how critical Earth system components such as permafrost and the Atlantic Meridional Overturning Circulation (AMOC) respond to and interact under warming. By using three climate models of varying complexity to assess the permafrost carbon response under idealized climate mitigation and overshoot scenarios, we here show that permafrost loses 11–21 PgC of carbon per 100 degree-years of warming exposure (cumulative warming over 100 years) during temperature overshoot in a robust linear relationship. This relationship also holds true under relative Northern Hemisphere cooling from a temporary AMOC slowdown during temperature overshoot. This relative cooling partially offsets climate change impacts on permafrost, while in itself causing adverse impacts on climate and society. These results underscore the importance of including both destabilizing and stabilizing Earth system feedbacks when assessing overshoot impacts, critical for informing carbon budgets, net-zero planning, and climate change reversibility.

Under current policies and pledges, overshooting 1.5 °C is almost certainly inevitable, as the majority of scenario pathways consistent with limiting global warming to 1.5 °C by the end of the century imply a temperature overshoot[1]. Such overshoot involves a temporary exceedance of the temperature goal, followed by the deployment of large-scale carbon dioxide removal (CDR) (Fig. 1a–c) to reach lower temperature levels. However, the extent to which a safe climate state could be reached after a temperature overshoot, and which processes triggered by the overshoot period might be irreversible, are both subject to uncertainty[2–4].

A prominent example for irreversible processes under climate change is the degradation of the permafrost carbon pool, which has been formed over thousands of years through the gradual accumulation of organic material in cold environments where decomposition is slow. An estimated 1460–1600 PgC (1 PgC = 1 GtC = 10^{15} gC) of permafrost carbon, with approximately 1000 PgC stored in the top 0–3 m of soil, is contained in the northern circumpolar region[5]. As permafrost thaws due to increasing global temperatures, soil microbes begin to decompose previously frozen soil organic matter, which releases carbon into the atmosphere. This process contributes to further warming and is known as the permafrost carbon-climate feedback. At present, northern permafrost regions experience higher warming than the global average due to Arctic amplification[6,7], and permafrost thaw is projected to further intensify toward the end of

[1]CICERO Center for International Climate Research, Oslo, Norway. [2]Bjerknes Centre for Climate Research, NORCE Norwegian Research Centre, Bergen, Norway. [3]Met Office Hadley Centre, Exeter, UK. [4]International Institute for Applied Systems Analysis (IIASA), Laxenburg, Austria. [5]Intelligent Earth UKRI AI Centre for Doctoral Training in AI for the Environment, University of Oxford, Oxford, UK. [6]School of Geography, University of Leeds, Leeds, UK. [7]School of Earth and Environmental Sciences, Seoul National University, Seoul, Republic of Korea. [8]Department of Biology, Norwegian University of Science and Technology, Trondheim, Norway. ✉e-mail: norman.steinert@cicero.oslo.no

 https://doi.org/10.1038/s41467-026-73612-0

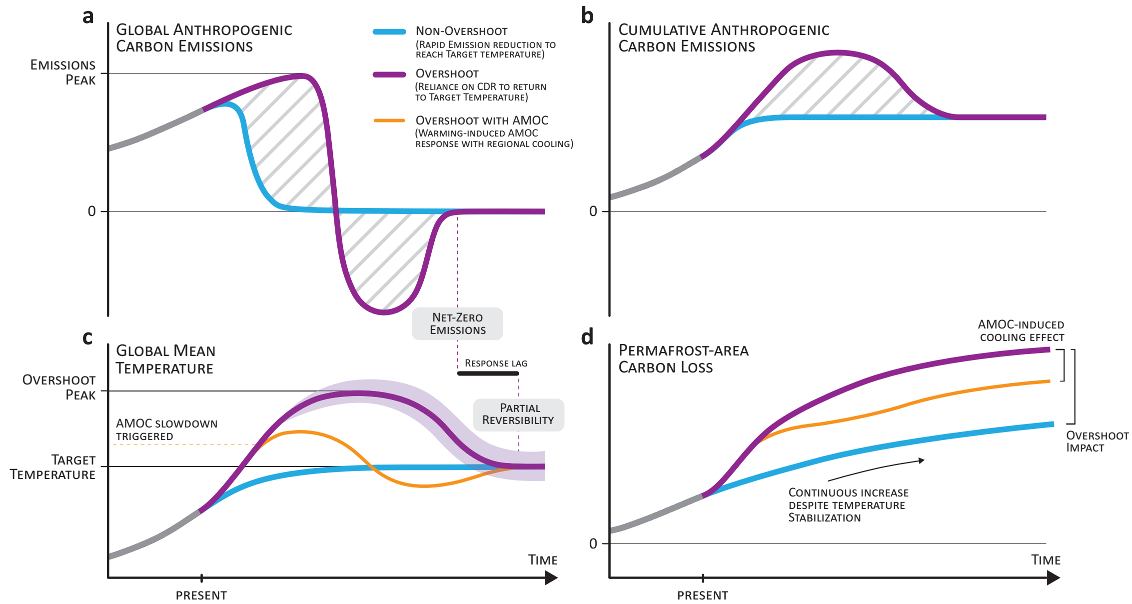

Fig. 1 | Conceptual illustration of permafrost carbon response in mitigation scenarios with and without slowdown of the Atlantic Meridional Overturning Circulation (AMOC). a, **b** Anthropogenic carbon emissions and cumulative carbon emissions without (blue) and with (purple) temporary overshoot, where the overshoot and the stabilization scenarios have the same final carbon budget. **c** Global mean temperature in response to the carbon emissions of the non-overshoot (blue) and overshoot (purple) pathways, with an additional case where an AMOC slowdown is triggered in response to the elevated temperatures during overshoot (orange). **d** Resulting permafrost carbon loss from the three scenarios. The stabilization scenario causes long-term permafrost carbon loss, which is enhanced under overshoot. With an additional AMOC response, permafrost carbon loss is reduced due to a stabilization from an AMOC-induced cooling of the permafrost region. Here, we aim to quantify the effect of AMOC-induced cooling on permafrost carbon loss.

the century[5,8,9]. Climate model simulations also suggest that the slow response of high-latitude soil carbon to climate warming will result in permafrost carbon loss that persists for centuries after a temperature stabilization[10,11].

The extent of carbon loss from permafrost depends on the trajectory of warming[12,13] and is therefore sensitive to the peak temperature and duration of temperature overshoot of climate mitigation pathways. The carbon release from permafrost during an overshoot is effectively irreversible, as there are no natural processes that can re-sequester it within centennial-to-millennial timescales. Modeling studies show that temperature overshoots lead to greater permafrost carbon release than scenarios that stabilize at a given temperature goal without exceeding it[10,11,13,14] (Fig. 1c, d).

The additional warming during a temperature overshoot may also decrease the strength, or even trigger the collapse, of the Atlantic Meridional Overturning Circulation (AMOC)[15–18]. The AMOC is a large system of ocean currents that transports heat northward in the Atlantic, but substantial warming and increased freshwater input from precipitation, river runoff, and ice melt, especially in the North Atlantic, can reduce upper-ocean density and weaken or even disrupt this circulation. Such AMOC slowdown would trigger a relative cooling (i.e., reduced warming) of the northern hemisphere high latitudes, producing the so-called North Atlantic warming hole[17,19–21]. This cooling enhances atmospheric stability and low cloud formation, increasing shortwave reflection and amplifying the regional cooling effect[22]. The reduced northward heat transport strengthens southern hemisphere ocean heat uptake (known as the bipolar seesaw), increasing total ocean heat storage and lowering global mean temperature (Fig. 1c). Such AMOC-induced cooling would alter temperature and precipitation patterns in Europe, and more widely across the northern hemisphere, which could disrupt marine and terrestrial ecosystems[17,23] and pose risks to food security[24]. Cooler regional climates might temporarily offset global warming but could also intensify extreme weather, such as temperature extremes in the North Atlantic region[25]. The resulting climatic changes would also impact infrastructure, and economic and political stability in affected regions[26].

Studies that examine the interactions between the AMOC and permafrost are rare[27–29]. For example, a recent review[30] assigned "very limited/missing evidence" to the strength and direction of the interaction between AMOC and permafrost carbon loss, as there is little evidence how permafrost thaw directly influences AMOC dynamics. Conversely, a weakening or collapse of the AMOC could induce regional cooling in the Arctic, potentially slowing permafrost thaw and reducing carbon emissions—a possible negative feedback on the permafrost carbon-climate feedback that has not been quantified yet. (Fig. 1d). Understanding this interplay is particularly important in the context of temperature overshoot scenarios, as both AMOC stability and permafrost carbon release are sensitive to the magnitude and duration of climate warming.

Here, we investigate how permafrost carbon responds to a set of experiments following idealized emission stabilization pathways, including scenarios with and without temperature overshoot of varying magnitude and duration (Fig. 2a)[11,17]. We consider four stabilization pathways, in which emissions are phased out after a cumulative total of 1500, 1750, 2000, or 2500 PgC has been emitted during the first 100 years[31]. We refer to these stabilization scenarios as B^x, where x denotes the cumulative carbon emissions in PgC. The lowest stabilization scenario B^{1500}, serves as a reference pathway, which reaches the level of 1500 PgC cumulative emissions without an overshoot. Overshoot trajectories branch off from the higher stabilization scenarios, eventually bringing cumulative carbon emissions down to 1500 PgC. We analyze a total of six overshoots by varying the branching time from the stabilization scenarios (either immediately or 100 years after positive emissions have ceased) and exceeding the reference level of 1500 Pg cumulative carbon emissions by 250, 500, and 1000 PgC, respectively. The six overshoot pathways are referred to as OS_y^x, with x indicating the cumulative amount of CDR in PgC and y indicating the duration of the overshoot—for example, OS_{100}^{250} being the overshoot with 250 Pg of carbon removal starting 100 years after the cessation of positive emissions.

https://doi.org/10.1038/s41467-026-73612-0

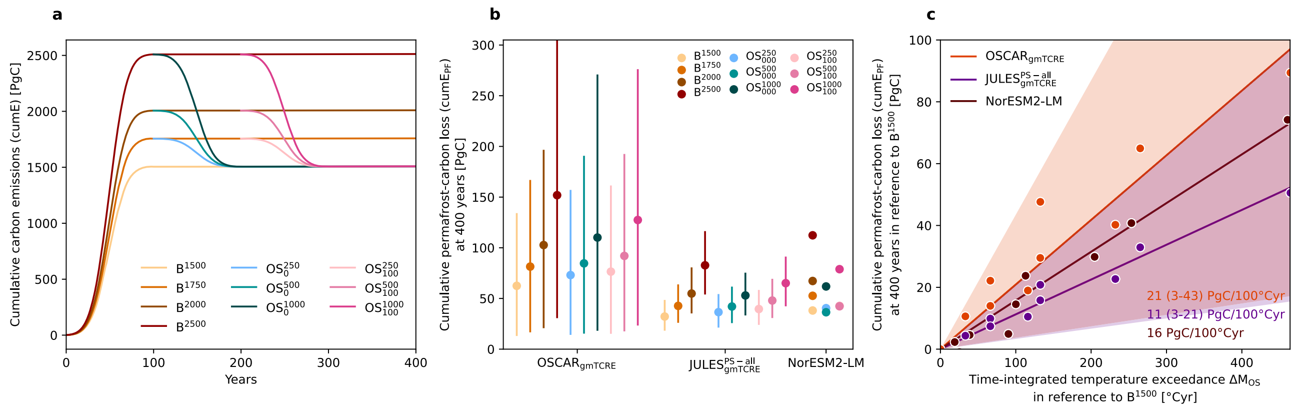

Fig. 2 | Linearity of permafrost carbon loss and warming exposure under temperature overshoot. a Cumulative anthropogenic carbon emissions profile of stabilization and overshoot scenarios following the Zero Emissions Commitment Model Intercomparison Project (ZECMIP[31]) protocol (see "Methods"). **b** Cumulative permafrost carbon loss at year 400 in simulations following the emission pathways shown in (**a**) with three models of different complexity (OSCAR, JULES, NorESM2-LM). Note that NorESM2-LM was run directly from emissions, whereas OSCAR and JULES were run with global mean temperatures derived from a linear transient climate response to cumulative emissions (TCRE; see "Methods"). Vertical bars denote uncertainty ranges from the simulation ensemble (minimum to maximum), depicting different model-dependent sources of uncertainty. **c** Relationship between the cumulative permafrost carbon loss and time-integrated temperature exceedance ($\Delta M_{OS} = M_{OS} - M_B$) in all scenarios as a difference to the B^{1500} stabilization reference scenario. Solid lines indicate a linear regression fit of the ensemble median per model for each scenario. Shaded areas, shown for OSCAR (orange) and JULES (purple), depict the spread of linear fits stemming from the ensemble spread in (**b**). Note that the upper bound of JULES's range coincides with OSCAR's median regression line at 21 PgC/100 °C yr, and that JULES's and OSCAR's lower bounds are almost identical at 3 PgC/100 °C yr.

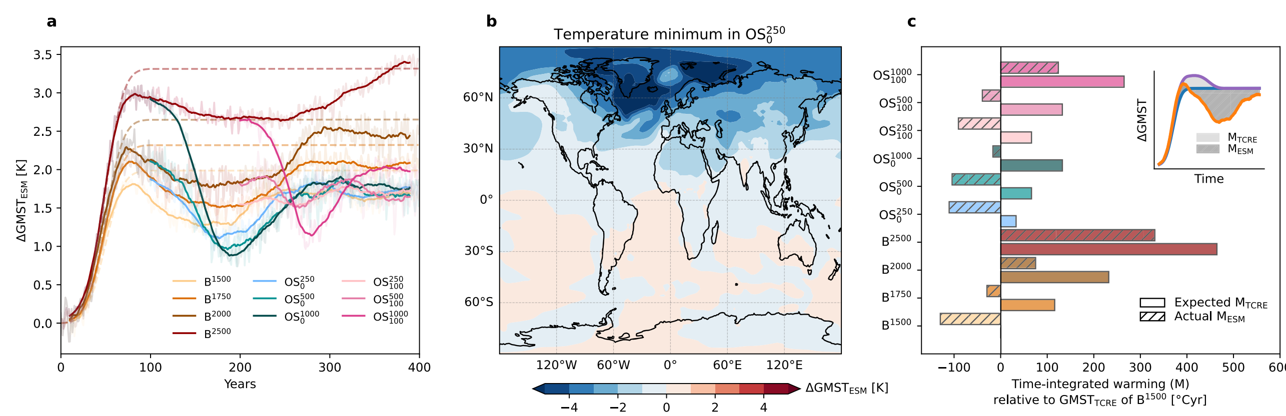

Fig. 3 | Regional cooling induced by the Atlantic Meridional Overturning Circulation (AMOC). a NorESM2-LM global mean temperature response to the cumulative emissions pathways in Fig. 2a for annual (pale solid lines) and 21-year running mean (solid lines) data. Dashed lines in the background indicate expected global mean surface temperatures (GMST) from a linear transient climate response to cumulative emissions (TCRE; $GMST_{TCRE}$) for the four stabilization scenarios for reference, and thus illustrate deviations of NorESM2-LM from this relationship. **b** Spatial temperature response as the difference between a state with reduced AMOC around the GMST minimum (years 180–190) and a state with stable AMOC and GMST (years 80–90) for the OS_0^{250} scenario, illustrating the high-latitude regional cooling imposed by the AMOC slowdown. **c** Time-integrated global mean temperatures (M; as illustrated in the top-right inset) per scenario relative to TCRE-derived temperatures of the B^{1500} scenario. Solid bars indicate temperatures expected from a linear TCRE relationship (expected M_{TCRE}; light gray shading in the inset). Striped bars indicate actual temperatures simulated by NorESM2-LM (actual M_{ESM}; dark gray shading in the inset). The difference between the respective bars denotes the time-integrated AMOC-induced cooling ΔM_{AMOC}. Note that the AMOC cooling can lead to time-integrated temperatures lower than the reference scenario, yielding negative numbers.

We use three models of different complexities to quantify the permafrost carbon response in these scenarios: NorESM2-LM—a full complexity Earth system model (ESM), JULES—a complex land surface model, and OSCAR—a compact ESM of reduced complexity (see "Methods" for a description of these models). This multi-model approach allows us to investigate the response of models representing a range of physical processes and their uncertainties and assess the robustness of our findings across model types. Among these models, NorESM2-LM is the only model representing an AMOC response to warming. NorESM2-LM shows a relatively high sensitivity of AMOC strength to warming, i.e., AMOC slows down quickly with small increases in temperatures (Fig. S1), and there is a pronounced relative cooling signal in global mean surface temperature (GMST) in the stabilization and overshoot scenarios (Fig. S2) as conceptualized in Fig. 1 (see also Fig. 3a, b, and ref. 17 for more details). NorESM2-LM's relatively strong AMOC decline in future scenarios[32] is consistent with, although at the upper end of the range of, a larger group of CMIP models showing at least moderate AMOC decline under warming[16,33]. The AMOC-related centennial GMST variations in our simulations lead to substantially cooler surface temperatures, particularly at northern high latitudes, compared to what is expected from the assumption of a constant GMST response to cumulative carbon emissions (TCRE)[34,35].

The effect of the AMOC cooling on permafrost carbon release is difficult to quantify with NorESM2-LM simulations alone because there is no counterfactual realization of NorESM2-LM without AMOC slowdown. We have therefore conducted additional experiments with

 https://doi.org/10.1038/s41467-026-73612-0

Table 1 | Experiment overview

ID	Experiment name ($model_{forcing}^{PatternScaling}$)	Forcing variable	Forcing variant	Pattern scaling	Output	Note
1	$OSCAR_{gmNorESM}$	Temperature	NorESM2-LM global mean	–	Global mean	AMOC cooling effect in global mean forcing
2	$OSCAR_{gmTCRE}$	Temperature	TCRE global mean	–	Global mean	–
3	$JULES_{spatialNorESM}$	Temperature	NorESM2-LM spatial	No	Spatial	Includes AMOC cooling pattern
4	$JULES_{gmNorESM}^{PS-all}$	Temperature	NorESM2-LM global mean	16 patterns	Spatial	AMOC cooling effect in global mean forcing
5	$JULES_{gmTCRE}^{PS-all}$	Temperature	TCRE global mean	16 patterns	Spatial	–
6	$JULES_{gmNorESM}^{PS-NorESM}$	Temperature	NorESM2-LM global mean	NorESM2 pattern	Spatial	AMOC cooling effect in global mean forcing
7	$JULES_{gmTCRE}^{PS-NorESM}$	Temperature	TCRE global mean	NorESM2 pattern	Spatial	–
8	NorESM2-LM	Emissions	–	–	Spatial	–

The naming convention for these experiments follows the notation $model_{forcing}^{PatternScaling}$, where (1) model can be NorESM2-LM, JULES or OSCAR, (2) PatternScaling, if indicated, denotes which type of pattern scaling was used, with either the average of 16 ESM patterns (PS—all, which includes the NorESM2 pattern) or the NorESM2 pattern alone (PS–NorESM), and (3) forcing denotes the forcing specification from global mean NorESM (gmNorESM) or TCRE-derived (gmTCRE) temperatures or forcing from spatial NorESM2-LM output fields (spatialNorESM). Note that this study does not represent all the feedback mechanisms quantified here in a fully coupled mode.

JULES and OSCAR (see "Methods") to extract the effects of the AMOC-induced relative cooling signal on permafrost carbon loss. We refer to these experiments following the notation $model_{forcing}^{PatternScaling}$ (Table 1), where (1) model can be NorESM2-LM, JULES or OSCAR, (2) PatternScaling, if indicated, denotes which type of pattern scaling was used, with either the average of 16 Coupled Model Intercomparison Project Phase 6 (CMIP6) model patterns (PS−all, which includes the NorESM2 pattern) or the NorESM2 pattern alone (PS−NorESM), and (3) forcing denotes the forcing specification from global mean NorESM (gmNorESM) or TCRE-derived (gmTCRE) temperatures, or forcing from spatial NorESM2-LM output fields (spatialNorESM). By using a combination of JULES and pattern scaling[36] with warming patterns derived from 16 CMIP6 ESMs covering a range climate sensitivities, we estimate uncertainties and establish the robustness of our results across a wide range of plausible climate responses. We do so similarly with OSCAR, which provides a wide coverage of uncertainty in permafrost-related parameterizations. First, these experiments are forced by idealized temperature pathways derived from a linear TCRE relationship following the emission pathways of our scenarios ($JULES_{gmTCRE}^{PS-all}$ and $OSCAR_{gmTCRE}$). Second, by forcing both models directly with global mean temperatures from the NorESM2-LM simulations ($JULES_{gmNorESM}^{PS-NorESM}$ and $OSCAR_{gmNorESM}$) and comparing them to the counterfactual experiments forced with idealized TCRE-derived global mean temperatures ($JULES_{gmTCRE}^{PS-NorESM}$ and $OSCAR_{gmTCRE}$), we obtain an estimate of how the AMOC cooling simulated in NorESM2-LM affects permafrost carbon loss in both of these models. For JULES specifically, we conduct an additional experiment ($JULES_{spatialNorESM}$) that uses spatially resolved climate output of NorESM2-LM, instead of the combination of global mean temperature and pattern scaling, to test the robustness of the results from global mean forcing against results where the spatially resolved temperature imprint of the AMOC slowdown is considered.

Results

Irreversible permafrost carbon loss under warming

Permafrost carbon loss derived from the three models (OSCAR, JULES, and NorESM) consistently increases with the level of anthropogenic carbon emissions and magnitude of the temperature overshoot in all models (Fig. 2b). The multi-model comparison reveals variations in the absolute magnitude of permafrost carbon loss, reflecting differences in how these models represent permafrost dynamics, soil carbon decomposition, and climate-carbon feedbacks. OSCAR shows both the strongest permafrost carbon response to warming and the largest ensemble spread (representing both model structural and climate sensitivity uncertainties; see "Methods"), covering estimates of JULES and NorESM on the lower end of its spread. JULES follows OSCAR's response pattern for each scenario, but the median permafrost carbon loss is smaller in magnitude. JULES's spread from the pattern scaling (depicting only climate uncertainty) is also much smaller. NorESM's response is more diverse, due to its more complex representation of climate variability and feedbacks, but generally agrees with the range of estimates simulated by JULES. The range of results across models indicates a model-complexity-dependent permafrost carbon response under warming.

The effect of temperature overshoot on permafrost carbon loss can also be seen across all models. Longer overshoot durations result in substantially higher permafrost carbon release, even if global temperatures return to lower levels eventually. The systematic increase in permafrost carbon loss with overshoot severity suggests that even short-lived temperature exceedance has long-lasting consequences for global carbon cycle feedbacks. This also implies that any prolonged exposure to higher temperatures leads to greater permafrost degradation than a no-overshoot stabilization scenario, and delaying temperature reversal (here simulated by a delay of 100 years) greatly amplifies the damage.

Despite the inter-model differences, a linear relationship emerges between the overshoot-induced cumulative warming exceedance over the B^{1500} scenario and cumulative permafrost carbon loss (time-integrated; Table S1) in all three models (Fig. 2c). Cumulative temperature exceedance ($\Delta M_{OS} = M_{OS} - M_B$) is the cumulative warming M (warming integrated over time; measured in degree-years °Cyr; Table S1) difference between the overshoot (M_{OS}) and its exceedance over the cumulative warming of the reference stabilization pathway (M_B). A quantification of this relationship for the three models gives: 21 (3–43) PgC/100 °C yr for OSCAR, 11 (3–21) PgC/100 °C yr for JULES, and 16 PgC/100 °C yr for NorESM. These values indicate that for every 100 °C yr of excess warming under overshoot, permafrost regions will release an estimated median range between models of 11 to 21 PgC/100 °C yr (absolute range of 3–43 PgC/100 °C yr). The linearity of this relationship remains robust across models and scenarios and implies that both the magnitude and duration of temperature overshoot are critical factors in determining the long-term permafrost carbon-climate feedback, but also that these factors might compensate for each other, i.e., a short but intense temperature overshoot is equivalent to a long temperature overshoot with a lower peak as long as the cumulative temperature exposure is identical.

AMOC-induced regional cooling reduces permafrost carbon loss

The implications of these findings extend beyond permafrost dynamics alone, as they intersect with other critical Earth system

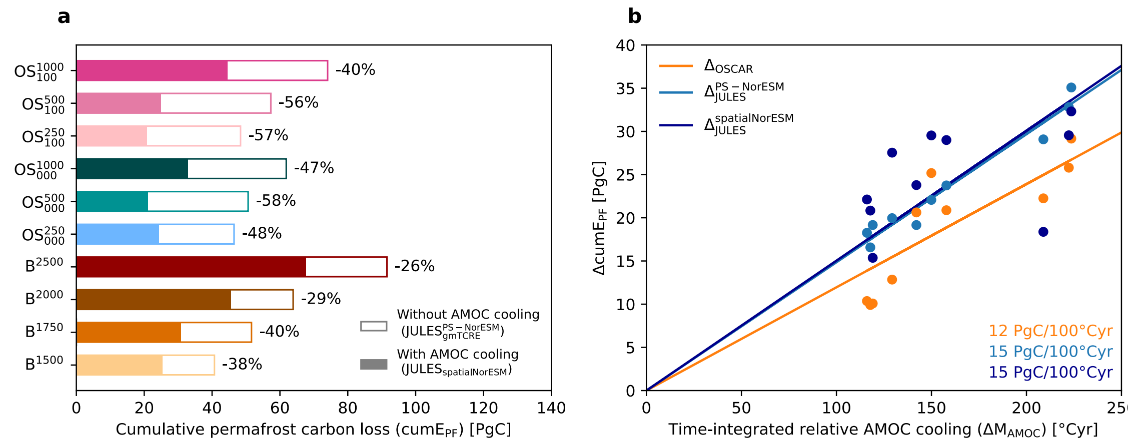

Fig. 4 | Atlantic Meridional Overturning Circulation (AMOC) effect on permafrost carbon loss. a Cumulative permafrost carbon response per scenario for $JULES^{PS-NorESM}_{gmTCRE}$ (white bars with colored borders; JULES without AMOC-induced cooling), and $JULES_{spatialNorESM}$ (colored bars; JULES with AMOC-induced cooling). The percentage reduction due to AMOC cooling is indicated next to the bars. **b** Relationship between the cumulative permafrost carbon loss difference ($\Delta cumE_{PF}$) and cumulative AMOC-induced cooling (difference between original and counterfactual simulations for OSCAR and two JULES variants) in all 10 scenarios. The three experiment combinations consist of:$\Delta_{OSCAR} = OSCAR_{gmTCRE} - OSCAR_{gmNorESM}$, $\Delta^{PS-NorESM}_{JULES} = JULES^{PS-NorESM}_{gmTCRE} - JULES^{PS-NorESM}_{gmNorESM}$, and $\Delta^{spatialNorESM}_{JULES} = JULES^{PS-NorESM}_{gmTCRE} - JULES_{spatialNorESM}$ (also see Table 1). Solid lines indicate the linear regression fit. Note that **a** shows the results for the two experiments associated with only one (dark blue) of the variants shown in (**b**).

elements, such as the AMOC. The linear dependence of permafrost carbon loss on temperature exposure under warming suggests that it also applies to any (relative) cooling scenario, which in turn is expected to reduce the rate of carbon release.

NorESM2-LM is well suited to address this hypothesis because it shows cooling relative to the expected temperature under the assumption of constant TCRE ($GMST_{TCRE}$; using NorESM2-LM's TCRE of 1.32 K/EgC derived from the concentration-driven 1pctCO2 simulation[37]) in all scenarios (Fig. 3a). The relative cooling is caused by an AMOC slowdown under warming (even without overshoot) that is intensified during temperature overshoot[17]. During positive anthropogenic emission phases, the strength of the AMOC declines by 48–76% from its preindustrial levels of 22.7 Sverdrup (Sv; Fig. S1). During the zero-emission phases, AMOC gradually recovers, stabilizing at a level slightly below its unperturbed state, with a difference of about 3–5 Sv, consistent with the range of previous studies[38]. Further, the AMOC recovery is accelerated under temperature overshoot (Fig. S1).

The AMOC-slowdown induces cooling due to reduced northward ocean heat transport and regional radiative feedbacks. The relative cooling significantly reduces the cumulative temperature exposure of permafrost regions between the expected temperatures from the TCRE relationship and actual temperatures from the ESM simulations (Figs. S3b and S4). The spatial pattern of the AMOC-induced cooling, consistent with other modeling studies[18,20], is centered around the North Atlantic but extends far into northern Eurasia and, to a lesser extent, northern North America, where large areas of permafrost are located (Fig. 3b), thereby leading to a lower integrated warming exposure of permafrost regions.

Although the AMOC does not permanently collapse in these NorESM2-LM simulations (Fig. S1), the recovery of the ocean circulation is a slow process. This induces a substantial cooling in stabilization scenarios, which is even stronger in the temperature overshoot scenarios (Fig. 3a, c). After emissions cease at year 100, the GMST evolution reflects: (1) declining radiative forcing as atmospheric carbon dioxide (CO_2) falls while land and ocean continue to absorb carbon, and (2) changes in ocean heat uptake. In many models, roughly constant post-emissions temperatures imply a balance between these two effects[31]. However, in NorESM2-LM, a strong AMOC decline increases ocean heat uptake enough to dominate the weakening radiative forcing, which produces continued cooling until AMOC recovery reduces ocean heat uptake and allows subsequent surface warming. In overshoot scenarios, the relative cooling is amplified because the reduction of the atmospheric CO_2 concentration due to idealized CDR is rapid and happens during a phase of reduced northward heat transport by the AMOC, before it can recover[17]. The time-integrated temperature exposure simulated by NorESM2-LM (M_{ESM}) is therefore substantially smaller than the time-integrated TCRE-derived temperature exposure (M_{TCRE}) for all scenarios (Fig. 3c). In the stabilization scenarios, M_{TCRE} is approximately 232 °C yr higher for each 500 Pg cumulative carbon emissions above the reference pathway. Further, the actual M_{ESM} is 129–172 °C yr cooler than the corresponding M_{TCRE} (Figs. 3c and S3). For example, the B^{1750} simulation, which is expected to be roughly 116 °C yr warmer than the reference pathway B^{1500} for M_{TCRE}, is actually cooler by 29 °C yr for M_{ESM}. In the overshoot scenarios, M_{TCRE} is larger for all overshoots, scaling with overshoot duration and magnitude. However, the actual M_{ESM}, which includes the effect of AMOC cooling, is lower than the expected M_{TCRE} for all overshoots, and even lower than the B^{1500} reference scenario for 5 out of 6 overshoots (the exception being the most extreme overshoot OS^{1000}_{100}).

Utilizing the specific JULES experiments (Table 1) allows to quantify the effect of the AMOC cooling on the magnitude of permafrost carbon loss. Permafrost carbon loss is substantially lower in the experiments with AMOC slowdown ($JULES_{spatialNorESM}$) than in the counterfactual experiments without AMOC slowdown ($JULES^{PS-NorESM}_{gmTCRE}$; Fig. 4a). These reductions range between 26 and 40% for the stabilization scenarios, and 40–57% for the temperature overshoot scenarios. For the overshoots, the largest difference in permafrost carbon loss can be found in the OS^{500}_{X} overshoot scenarios, correlating with the strongest AMOC slowdown relative to the warming in these scenarios (Fig. S3). These results indicate that AMOC-induced cooling provides a stabilizing effect on permafrost carbon loss by lowering regional temperatures and reducing permafrost thaw and associated carbon release. In turn, such a reduction in permafrost carbon loss is expected to weaken the permafrost carbon-climate feedback strength.

The reductions in permafrost carbon loss due to AMOC cooling decrease in high-emission scenarios, driven by two mechanisms. Firstly, the AMOC weakening response to warming has a maximum rate at a specific temperature range (around 2–2.5 °C, equivalent to emissions in B^{2000} and OS^{500}_{X} in NorESM2-LM; see Figs. 3 and S3).

 https://doi.org/10.1038/s41467-026-73612-0

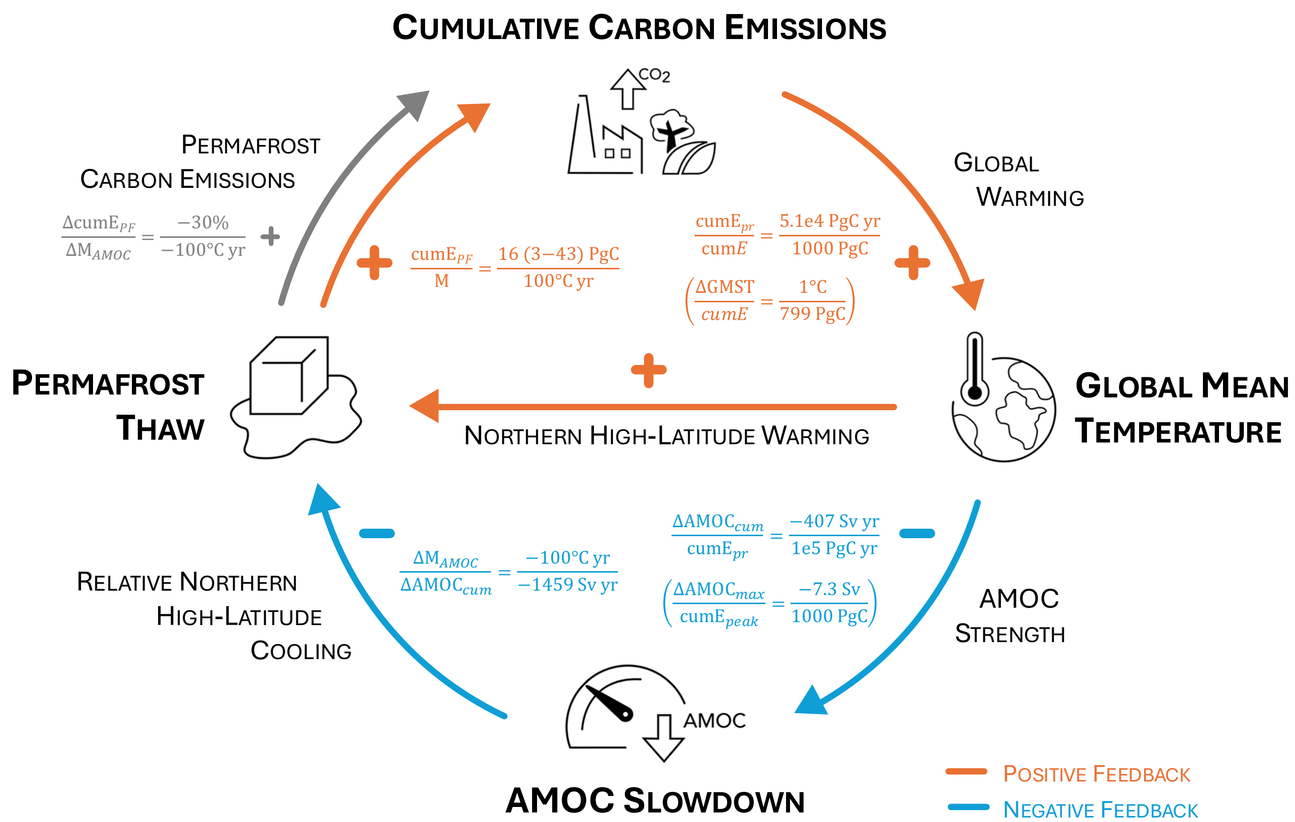

Fig. 5 | AMOC cooling impact on permafrost carbon. Conceptual feedback diagram of the common permafrost carbon-climate feedback (positive feedback; orange loop) and the stabilizing AMOC-induced cooling effect (negative feedback; blue loop). While the effect of an AMOC slowdown decreases the permafrost carbon-climate feedback strength, the latter remains effectively positive under the warming scenarios discussed here. Note that the feedback numbers provided here do not represent all the feedback mechanisms in a fully coupled mode.

Secondly, the strength of the AMOC effect on permafrost depends on the strength of the AMOC slowdown in relation to the warming that causes it. Importantly, there is an absolute limit for the cooling capacity of the AMOC. Once the warming is large enough to trigger a complete collapse of the AMOC, further warming will not induce further relative cooling. It is therefore important to emphasize that rapid emission reductions is the most effective way to protect permafrost carbon integrity.

Subtracting the original and the counterfactual experiments for each scenario yields the permafrost carbon loss difference ($\Delta cumE_{PF}$) in relation to the time-integrated AMOC cooling ($\Delta M_{AMOC} = M_{TCRE} - M_{ESM}$). The permafrost carbon loss difference shows a general trend where larger cumulative AMOC-induced cooling corresponds with lower cumulative permafrost carbon loss (Fig. 4b, see Table 1 and the "Methods" section for experiment details). Assuming a linear relationship, we find a median AMOC-induced reduction of permafrost carbon loss of 12 PgC/100 °C yr for OSCAR (Δ_{OSCAR}), and 15 PgC/100 °C yr for two JULES variants ($\Delta_{JULES}^{PS-NorESM}$, and $\Delta_{JULES}^{spatialNorESM}$). These results are in good agreement with the relationship derived under positive warming changes (Fig. 2) and support its applicability under relative cooling. Due to the large temporal and spatial variability of the regional climate response to the AMOC collapse and the complexity of the permafrost responses to the temperature forcing in NorESM, there can be deviations from that relationship among individual simulations. However, the linear fit improves when using the pattern scaling approach with the NorESM2-LM global mean temperature response instead of the spatially and temporally resolved NorESM2-LM temperature to force JULES (compare the light blue and dark blue dots). The relationship is robust also against other methodological variations (Fig. S4).

Quantifying the AMOC-slowdown effect on permafrost carbon loss

The interaction between AMOC cooling effects and the permafrost carbon-climate feedback exhibits positive and negative feedback loops impacting the global climate (Fig. 5). For NorESM2-LM, each 799 PgC of cumulative anthropogenic carbon emissions leads to 1 °C of global warming (Figs. 5 top right, S5). Subsequently, this warming causes permafrost carbon loss of 16 (3–43) PgC/100 °C yr (Fig. 2). This carbon release can intensify the greenhouse effect via the permafrost carbon-climate feedback, further warming the atmosphere, which in turn speeds up permafrost thaw and amplifies greenhouse gas release, perpetuating a self-reinforcing cycle that drives continued global warming (Fig. 5, orange loop).

We have shown here that this positive climate feedback loop can be weakened by reduced permafrost carbon loss as a consequence of relative cooling induced by an AMOC slowdown in response to anthropogenic carbon emissions. In NorESM2-LM, the AMOC is weakened under global warming (Fig. S2), and its maximum decline ($\Delta AMOC_{max}$) is generally well correlated with the cumulative anthropogenic emissions peak ($cumE_{peak}$) of each scenario (Fig. S6), which yields a maximum AMOC decline of 7.3 Sv per 1000 PgC of cumulative emissions (Fig. 5, bottom right). However, $cumE_{peak}$ and $\Delta\ AMOC_{max}$ do not account for any temporal variations of the AMOC, such as its accelerated recovery under temperature overshoot. Particularly after substantial weakening of the AMOC and eventual stabilization of emissions in all scenarios, this relationship between cumulative emissions and AMOC strength becomes highly nonlinear or even decoupled. This is illustrated by a scenario-pathway dependent correlation of the cumulative AMOC decline ($\Delta AMOC_{cum}$; AMOC change integrated over time; units: Sv yr) with $cumE_{peak}$ (Fig. S6), which is why the latter is a weak predictor for the overall impact of the AMOC slowdown over time. We therefore argue that the integral-based estimates provide a more robust quantification of these relationships. Hence, to fully account for AMOC's temporal evolution (both the magnitude and duration) in the estimate of warming impact on the AMOC, we consider the cumulative emissions pressure $cumE_{pr}$ (integrated cumulative emissions over time; 5.1×10^4 PgC yr per 1000 PgC of cumulative emissions; see Figs. 5 top right, S5, and Table S1) and the cumulative AMOC decline $\Delta AMOC_{cum}$ as proxies for systemic forcing. Per 1×10^5 PgC yr of $cumE_{pr}$, there is an integrated AMOC slowdown of −407 Sv yr (Fig. 5, bottom right). In turn, this metric can be used to estimate the AMOC-induced relative cooling from this slowdown (ΔM_{AMOC}; Fig. S7), which yields −100 °C yr per −1459 Sv yr of integrated AMOC slowdown (Fig. 5 bottom left). Note that this relationship is compromised in the highest emission scenarios B^{2500} and OS_x^{1000}, presumably because of interfering climate feedback effects on the global mean temperature that lead to smaller than expected integrated AMOC-induced cooling, which is why we omitted them in the quantification of this step of the feedback loop (Fig. S7). The relative cooling is particularly strong in the northern high latitudes (Fig. 3), such that the thawing process of permafrost is slowed down. With fewer emissions contributing to the permafrost carbon-climate feedback, warming slows, creating a stabilizing effect on temperatures that can partially slow down further climate warming. This stabilizing AMOC effect on permafrost carbon loss from these regions leads to a 30% reduction of permafrost carbon loss per 100 °C yr of AMOC-induced relative cooling (Figs. 5, bottom right, S8). It should be noted that, while this effect can partially offset further climate warming from the permafrost carbon-climate feedback, it does not halt or even reverse global warming, and it neither would protect from any climate change impacts that would manifest under any of the considered warming scenarios. On the contrary, the AMOC slowdown itself brings many adverse impacts on climate[39,40], environment, society, and economy[24,26].

By quantifying each step in the feedback loop between cumulative anthropogenic carbon emissions, AMOC changes, and permafrost carbon loss, this study enables estimation of the permafrost carbon loss under (cumulative) warming, and equally, the reduction of permafrost carbon loss from (cumulative) AMOC-induced cooling, directly from cumulative emission pathways, while taking into account the uncertainties in each step of the feedback loop. For example, the OS_{100}^{250} scenario, a moderate emissions overshoot of a duration of 100 years, exerts 5.8×10^5 PgC yr of cumulative emissions pressure, which yields a reduction of permafrost carbon loss of 57% due to AMOC-induced cooling - an overestimation of 9% to the actual calculation of this feedback effect in this specific scenario (Table S2 and Fig. 4). Further estimates of this feedback loop are robust across all scenarios, although the generalization provided here applies less to the stabilization and overshoot scenarios based on 2500 PgC of peak cumulative emissions because of the smaller than expected integrated AMOC-induced cooling is these scenarios (Table S2). Note that this study does not represent all the feedback mechanisms in a fully coupled mode. Regardless, our analysis provides useful insights into the direction and strength of the effect of an AMOC slowdown on permafrost carbon in a warming climate.

Discussion

Here, we explore the interaction between the AMOC and permafrost, both widely considered as key Earth system components and potential tipping elements, in idealized climate mitigation scenarios using three models of varying complexity. Across all models, we find a robust, linear relationship between permafrost carbon loss and cumulative warming exposure under overshoot of 11–21 PgC per 100 °C yr, indicating that even temporary temperature overshoots lead to long-lasting and effectively irreversible permafrost carbon release. The extent of permafrost carbon release depends on both the peak temperature and the duration of warming, suggesting that longer and higher overshoots cause more significant permafrost carbon loss. Hence, the duration and magnitude of temperature exceedance, not just peak warming, are critical determinants of long-term carbon cycle feedbacks, which underscores the importance of minimizing any exceedance of temperature targets.

The effect of cumulative warming exposure on permafrost carbon loss also applies in scenarios of relative cooling due to an AMOC slowdown. We estimate that permafrost carbon loss is reduced by up to 40% in zero-emission stabilization scenarios and up to 60% in overshoot scenarios when temporary AMOC weakening leads to cooling over the permafrost region. This effect scales approximately linearly with the magnitude of this cooling and partially counteracts the permafrost carbon-climate feedback. While this process slows down carbon release, it does not reverse permafrost degradation or restore carbon already emitted. Although NorESM2-LM shows a comparatively strong AMOC sensitivity to warming, and therefore potentially overestimates the absolute effects of AMOC cooling on the reduction of permafrost carbon loss, we describe and quantify a general feedback mechanism that is applicable to any future emission pathway where AMOC's response to warming is variable. While the AMOC-induced cooling reduces the permafrost carbon-climate feedback, it should be noted that an AMOC slowdown in itself will shift regional climate patterns and increase the risk of extreme events, which might subsequently threaten food and water security and may cause economic and geopolitical instability in affected regions[17,23,24,26].

Further warming or temporary exceedance of a climate warming limit may lead to a potentially "quiet" contribution of Arctic carbon emissions due to permafrost thaw, given that the permafrost carbon-climate feedback is still not well represented in many climate assessments[14,41]. The absence of the permafrost carbon-climate feedback in climate models likely leads to an overestimation of the remaining carbon budget for achieving specific global warming targets[13,42]. Including the permafrost carbon-climate feedback could reduce the remaining carbon budgets for staying below warming targets, such as 1.5 or 2 °C. In turn, the existence of a negative AMOC effect on permafrost, not considered in previous carbon budget estimates, means a refined contribution of the permafrost carbon-climate feedback to these estimates.

The quantification of the AMOC effect on permafrost provided here is not a closed feedback loop, as the reduced permafrost carbon loss does not interactively feed back to the climate in our simulations. Future research should incorporate this coupling and refine the permafrost-carbon representation in climate models to incorporate these findings into climate projections that support long-term climate change mitigation strategies. For example, our results, obtained from more complex models, can inform the implementation of the permafrost carbon-climate feedback in simple climate models and models of intermediate complexity that intend to resolve climate tipping dynamics[43]. By integrating functions of the permafrost carbon response to cumulative warming and overshoot-dependent emissions, combined with the AMOC effect on permafrost, simple climate models can provide more realistic projections of future warming and mitigation efforts. Such efforts could also be crucial for designing climate policies and scenarios, and ensuring more accurate predictions of long-term climate trajectories from processes that are yet difficult to represent (e.g., permafrost carbon loss to warming[14,41,44]) or to model (e.g., AMOC slowdown[32,45,46]) in more complex climate models, such as ESMs.

Situated at the intersection of AMOC dynamics, climate mitigation, carbon-climate feedbacks, and tipping point research, this study establishes a linear relationship between temperature exposure and permafrost carbon loss. While permafrost carbon release is often nonlinear at local scales because abrupt thaw features, such as thermokarst lakes, can trigger strong initial emissions pulses[47], the aggregated pan-Arctic scale response is expected to still appear roughly proportional to warming in current assessments[44,48]. Currently, there is no clear evidence that Arctic permafrost shows tipping-like behavior even under high-magnitude warming and extended time scales. However, because current climate models still represent permafrost structure, physics, and carbon dynamics poorly, and centennial climate projections beyond 2100 remain uncertain, large-scale abrupt permafrost change at high temperature levels (e.g., above 5 °C global warming[44]) or multi-centennial time scales cannot be ruled out completely either.

The emergent permafrost-warming dependency shown here allows to quantify the effects of temperature-modifying processes triggered by climate change on permafrost carbon pools, and thus fills a critical gap by explicitly assessing the missing interactions between major climate tipping elements[30]. The AMOC response analyzed here reflects the current scientific debate and uncertainty regarding a potential near-future slowdown and its impacts[49–51]. Equally, permafrost is expected to experience irreversible carbon loss under any warming scenario, and especially under overshoot[2,10,52–54]. While previous studies have examined these systems largely in isolation, our results create a link between future AMOC changes and permafrost response and how AMOC weakening and recovery modulate regional and global temperatures, and thereby influence the timing and magnitude of permafrost carbon release. Neglecting such interactions could misrepresent long-term warming risks, carbon-cycle feedbacks, and the challenges of achieving climate stabilization after an overshoot. The established permafrost-warming relationship also allows to infer that, if temporary cooling from carbon storage in nature[55] or peak-shaving from geoengineering[56] would be able to reduce overshoot warming, this can be directly translated into a reduction in permafrost carbon loss.

The results presented here underscore the urgency of limiting global temperature overshoots rather than relying on CDR to compensate for excessive anthropogenic carbon emissions. Further, the interplay between these positive and negative climatic feedbacks demonstrates the sensitivity of climate systems, where fluctuations in AMOC strength can significantly affect permafrost stability and greenhouse gas emissions. The strong coupling between AMOC variability and the permafrost carbon response demonstrates that transient circulation changes can mask or amplify warming over different timescales, adding uncertainty to the climate response during and after overshoot periods. Given the irreversible nature of permafrost carbon loss and the uncertainties surrounding AMOC's response to warming, policymakers should prioritize strategies that minimize time-integrated temperature exposure, i.e., lower overshoot peak temperature and shorter duration, to reduce long-term risks. Our results are critical for understanding the interplay between ocean circulation changes and carbon cycle feedbacks in a warming world, especially where tipping points and long-term carbon budgets are concerned. Incorporating these coupled tipping-element dynamics into carbon budget assessments and CDR planning is essential to avoid underestimating future warming, carbon feedbacks, and the societal and ecological costs of delayed mitigation. AMOC stability thus emerges as a crucial factor in modulating climate change impacts, where its overall effect on permafrost carbon loss depends on the level of warming, and the duration and magnitude of the temperature overshoot, underscoring the importance of early and sustained emission reductions to limit cascading Earth system responses.

Methods

OSCAR

We utilize the compact Earth system model OSCARv3.1.2[57], which incorporates parameterizations for permafrost thaw, soil organic matter decomposition, and CO_2 and CH_4 emissions since version v2.2.1[13]. The OSCAR's permafrost carbon module specifically addresses high-latitude processes. Its climate response is tuned to 21 ESMs from CMIP6, its permafrost carbon response is calibrated on five advanced land surface models (JSBACH, ORCHIDEE-MICT, and JULES-DeepResp, JULES-SuppressResp, UVic), and is further scaled up to match the low- or high-end estimates of the initial permafrost carbon pool size from the IPCC SROCC[58]. The permafrost carbon module offers a 210-member ensemble for global permafrost carbon loss, with its uncertainty range representing the differences in land surface models capable of simulating the permafrost system, as well as differences in climate response. The parameters for the permafrost module were calibrated for North America and Eurasia using outputs from complex models over the period 1850–2300 under RCP scenarios 8.5, 4.5, and 2.6[13]. Permafrost carbon refers to the carbon pool that was frozen and therefore inactive during preindustrial times. The permafrost carbon pools change over time according to the thawing carbon flux. This flux is calculated as the product of the preindustrial size of the frozen pool and the rate of change of the currently thawed fraction calibrated by the land surface model's thawing carbon fluxes and heterotrophic respiration rates, and driven only by the temperature change taken from the emulated land surface model.

JULES

The Joint UK Land Environment Simulator (JULES[59,60]) is the land surface component of the UK Earth System Model (UKESM) and is used herein to simulate the set of ten climate change scenarios. JULES is a model that simulates the physical, biophysical, and biochemical processes governing the exchange of radiation, momentum, heat, water, and carbon between the land surface and the atmosphere. JULES models the terrestrial response to changes in these climate variables, with each grid point representing multiple land-cover types and non-vegetated areas. The surface energy balance is calculated based on the fractional coverage of these land types within a grid, although the underlying soil is treated as a single column that receives aggregated mean fluxes.

Here, we use a permafrost-adapted version of JULES[61,62]. To enhance the representation of physical and biogeochemical processes in cold regions, several key modifications have been incorporated into JULES. These include updated soil thermal and hydraulic properties to consider the presence of organic matter and a vertically resolved soil carbon decomposition. The model supports a deeper and more finely resolved soil column for the simulation of thermal, hydrological, and biogeochemical processes, with 20 layers nodes increasing in thickness from 0.65 m at the surface to 5 m at the deepest level, reaching a total soil column depth of 7.2 m. Below this depth, a thermal column represents bedrock, where only thermal processes are simulated. The standard model configuration, typically used in UKESM, also includes a dynamic vegetation component that simulates vegetation distribution and its response to climate change. However, for the purpose of this study, dynamic vegetation is turned off, as it offsets some of the permafrost carbon loss by increasing soil carbon input from vegetation growth in thawed permafrost areas under warming. Since neither OSCAR nor NorESM2-LM represents dynamic vegetation, this also enhances comparability between models. Regardless, we note that processes, such as dynamic vegetation or nitrogen fertilization may enhance the simulated carbon sink and can therefore reduce the permafrost carbon-climate feedback.

NorESM2-LM

NorESM2[63,64] is based on the Community Earth System Model (CESM2.1)[65] and employs the original land (CLM5) and sea-ice (CICE) components as well as the coupling infrastructure of CESM2.1. The atmospheric component is CAM6 (as in CESM) but with modifications regarding the energy and angular momentum conservation, and a different atmospheric aerosol module. The ocean physical and biogeochemical components of NorESM2 are the isopycnal ocean circulation and carbon cycle components updated from NorESM1[66,67]. The model has contributed to the CMIP6, and is used here in the configuration with 1 degree resolution in the ocean/sea-ice components and 2 degree resolution in the atmosphere/land components (NorESM2-LM). NorESM2-LM includes atmospheric, oceanic, sea ice, and land surface components and incorporates an advanced carbon-cycle representation. It is particularly suited for studying feedbacks between the ocean, atmosphere, biosphere, and cryosphere, including complex interactions related to carbon emissions and climate dynamics. For the simulations provided here, solely CO_2 emissions are considered as the forcing factor, while land use and non-CO_2 greenhouse gas forcings are kept at pre-industrial levels[11].

NorESM2-LM has run three initial condition ensemble members for each of the stabilization and overshoot pathways in emission-driven mode (see ref. 17 for more details). With 22.7 Sv at 40°N, NorESM2-LM is among the CMIP6 models with a stronger-than-observed contemporary overturning strength (CMIP6 range: 9.6–23 Sv; mean: 17.7 Sv, observation-based estimate 17.4 Sv)[32], and it tends to simulate a strong decline in AMOC strength with climate change.

Pattern scaling

To generate projections of regional climate impacts on permafrost on the spatially resolved grid in JULES from the idealized TCRE-derived global mean temperature ($GMST_{TCRE}$) and NorESM2-LM global mean temperature ($GMST_{ESM}$) time series, we make use of pattern scaling as in ref. 36 to derive climate forcing for the JULES land surface model. An early form of pattern scaling methodology[68,69] is followed to emulate the response of 16 CMIP6 ESMs, sampling the CMIP6 ensemble's range of uncertainty. For each ESM, monthly linear relationships are derived between the global mean temperature anomaly (relative to the 1850–1889 mean) and eight variables (near-surface air temperature, diurnal temperature range, near-surface specific humidity, 10 m wind speed, surface pressure, precipitation, surface downwelling shortwave radiation, and surface downwelling longwave radiation)[36] at each grid cell using the SSP5-8.5 climate scenario[70]. Wells et al.[71] show that the best all-round emulation performance is achieved by using a high warming scenario to obtain the patterns, hence our choice of SSP5-8.5 as the training scenario. We then use the IMOGEN code[72] (as part of JULES) to generate hourly data, simulate the diurnal cycle and exchange of heat, water, and momentum; this is similar to the disaggregator described in ref. 73. These patterns are scaled by $GMST_{TCRE}$ or $GMST_{ESM}$ profiles are then used to drive JULES and return the permafrost carbon loss. We note that the temperature patterns (and those of other climate variables) used for the pattern-scaling approach contain little, if any, imprint of the AMOC slowdown, since they are derived from transient warming simulations over a relatively short time span of 85 years (2015–2100; Fig. S9). The climate patterns used here can be reproduced using ESMValTool with the pattern recipe, including automatic downloads of the required CMIP6 data from ESGF[74].

Scenario design

The carbon emissions in the B-simulations are described by idealized bell-shaped curves, with 50 years of increasing emissions followed by 50 years of decreasing emissions, following the Zero Emissions Commitment Model Intercomparison Project (ZECMIP) protocol[75]. Negative cumulative emission trajectories exhibit a similar pattern but with negative values. In the stabilization scenarios B^{1500}, B^{1750}, B^{2000}, and B^{2500}, cumulative carbon emissions amount to 1500, 1750, 2000, and 2500 PgC during the initial 100 years, followed by zero emissions for the subsequent 300 years. The reference simulation B^{1500} of 1500 PgC of cumulative emissions results in a long-term global warming level of approximately 1.7 °C in NorESM2-LM due to its low transient climate response to cumulative emissions (TCRE) of 1.32 K/EgC[37]. For the overshoot simulations, the emission trajectories involve the same emissions profile as the stabilization scenarios for the first 100 years, followed by the application of CDR, assumed here as idealized negative emissions, which removes 250, 500, and 1000 PgC over another 100 years. CDR is applied in two different periods, one starting immediately after peak emissions are reached in year 100, and one after emission stabilization was maintained for 100 years. Following the cessation of negative emissions, the scenarios enter an extended phase of 200 and 100 years of zero emissions, respectively, resulting in identical cumulative carbon emissions as in B^{1500} for these periods. This setup gives 4 stabilization and 6 overshoot scenarios, and allows analyzing climate system responses under clearly defined overshoot trajectories, including overshoots of different magnitudes and durations and different rates of CDR applied. Land-use and non-CO_2 forcings are kept constant at pre-industrial levels.

Simulation experiment setups

Various simulation experiment setups and forcing variants were used to simulate the response of permafrost carbon to warming and to extract the effects of AMOC-induced cooling on permafrost carbon loss (Table 1). NorESM2-LM served as a reference for spatially explicit atmospheric conditions and AMOC behavior. Since there is no counterfactual simulation of NorESM with a stable AMOC under warming, we conduct simulations with JULES in standalone mode using several variants: (1) $JULES^{PS-all}_{gmTCRE}$, driven by global mean temperature time series derived from a linear TCRE relationship ($\Delta GMST_{TCRE}$) using pattern scaling based on 16 CMIP6 models; (2) $JULES^{PS-all}_{gmNorESM}$, using global mean temperatures from NorESM2-LM with pattern scaling (all 16 patterns) to preserve AMOC-induced effects; (3 and 4) same as (1 and 2) but using only the NorESM climate pattern for the pattern scaling ($JULES^{PS-NorESM}_{gmTCRE}$ and $JULES^{PS-NorESM}_{gmNorESM}$); and (5) $JULES_{spatialNorESM}$, using the full spatial temperature output from NorESM2-LM (without pattern scaling). OSCAR simulations were similarly run with two forcing setups: (1) $OSCAR_{gmTCRE}$, forced by global mean temperatures assuming constant TCRE, and (2) $OSCAR_{gmNorESM}$, forced directly by global mean temperature from NorESM2-LM simulations. Subtracting the experiments with AMOC-induced cooling and the counterfactual experiments without AMOC-induced cooling yields the permafrost carbon loss difference in relation to the time-integrated AMOC cooling. Here, we subtract $JULES^{PS-all}_{gmTCRE}$ and $JULES^{PS-all}_{gmNorESM}$, $JULES^{PS-NorESM}_{gmTCRE}$ and $JULES^{PS-NorESM}_{gmNorESM}$, and $JULES^{PS-NorESM}_{gmTCRE}$ and $JULES_{spatialNorESM}$ to provide results for various experiment variants of JULES. We do the same for OSCAR by subtracting $OSCAR_{gmTCRE}$ and $OSCAR_{gmNorESM}$.

Data availability

All data to reproduce the analyses and figures are available via figshare at https://doi.org/10.6084/m9.figshare.30710540[76].

Code availability

Python notebooks, together with the Python environment, to reproduce the analyses and figures, are available via figshare at https://doi.org/10.6084/m9.figshare.30710540[76].

References

1. Meinshausen, M. et al. Realization of Paris Agreement pledges may limit warming just below 2 °C. *Nature* **604**, 304–309 (2022).
2. Schleussner, C.-F. et al. Overconfidence in climate overshoot. *Nature* **634**, 366–373 (2024).
3. Pfleiderer, P., Schleussner, C.-F. & Sillmann, J. Limited reversal of regional climate signals in overshoot scenarios. *Environ. Res. Clim.* **3**, 015005 (2024).
4. Steinert, N. J., Schwinger, J., Chadwick, R., Kug, J.-S. & Lee, H. Irreversible land water availability changes from a potential ITCZ

shift during temperature overshoot. *Earth's Future* **13**, e2024EF005787 (2025).
5. Schuur, E. A. G. et al. Permafrost and climate change: carbon cycle feedbacks from the warming Arctic. *Annu. Rev. Environ. Resour.* **47**, 343–371 (2022).
6. Rantanen, M. et al. The Arctic has warmed nearly four times faster than the globe since 1979. *Commun. Earth Environ.* **3**, 168 (2022).
7. Watts, J. D. et al. Regional hotspots of change in northern high latitudes informed by observations from space. *Geophys. Res. Lett.* **52**, e2023GL108081 (2025).
8. Biskaborn, B. K. et al. Permafrost is warming at a global scale. *Nat. Commun.* **10**, 264 (2019).
9. Nissan, A. et al. Global warming accelerates soil heterotrophic respiration. *Nat. Commun.* **14**, 3452 (2023).
10. Vrese, P. D. & Brovkin, V. Timescales of the permafrost carbon cycle and legacy effects of temperature overshoot scenarios. *Nat. Commun.* **12**, 2688 (2021).
11. Schwinger, J., Asaadi, A., Steinert, N. J. & Lee, H. Emit now, mitigate later? Earth system reversibility under overshoots of different magnitudes and durations. *Earth Syst. Dyn.* **13**, 1641–1665 (2022).
12. Burke, E. J., Chadburn, S. E., Huntingford, C. & Jones, C. D. CO2 loss by permafrost thawing implies additional emissions reductions to limit warming to 1.5 or 2 °C. *Environ. Res. Lett.* **13**, 024024 (2018).
13. Gasser, T. et al. Path-dependent reductions in CO_2 emission budgets caused by permafrost carbon release. *Nat. Geosci.* **11**, 830–835 (2018).
14. Natali, S. M. et al. Permafrost carbon feedbacks threaten global climate goals. *Proc. Natl. Acad. Sci. USA.* **118**, e2100163118 (2021).
15. Pontes, G. M. & Menviel, L. Weakening of the Atlantic Meridional Overturning Circulation driven by subarctic freshening since the mid-twentieth century. *Nat. Geosci.* **17**, 1291–1298 (2024).
16. Bonan, D. B. et al. Observational constraints imply limited future Atlantic Meridional Overturning Circulation weakening. *Nat. Geosci.* **18**, 479–487 (2025).
17. Schwinger, J., Asaadi, A., Goris, N. & Lee, H. Possibility for strong northern hemisphere high-latitude cooling under negative emissions. *Nat. Commun.* **13**, 1095 (2022).
18. Romanou, A. et al. Stochastic bifurcation of the North Atlantic circulation under a midrange future climate scenario with the NASA-GISS ModelE. *J. Clim.* **36**, 6141–6161 (2023).
19. Bellomo, K., Angeloni, M., Corti, S. & Hardenberg, J. V. Future climate change shaped by inter-model differences in Atlantic Meridional Overturning Circulation response. *Nat. Commun.* **12**, 3659 (2021).
20. Bellomo, K. & Mehling, O. Impacts and state-dependence of AMOC weakening in a warming climate. *Geophys. Res. Lett.* **51**, e2023GL107624 (2024).
21. Lee, Y.-C., Liu, W., Fedorov, A. V., Feldl, N. & Taylor, P. C. Impacts of Atlantic Meridional Overturning Circulation weakening on Arctic amplification. *Proc. Natl. Acad. Sci. USA.* **121**, e2402322121 (2024).
22. Laurian, A., Drijfhout, S. S., Hazeleger, W. & van den Hurk, B. Response of the western European climate to a collapse of the thermohaline circulation. *Clim. Dyn.* **34**, 689–697 (2010).
23. Boot, A. A., Steenbeek, J., Coll, M., von der Heydt, A. S. & Dijkstra, H. A. Global marine ecosystem response to a strong AMOC weakening under low and high future emission scenarios. *Earth's Future* **13**, e2024EF004741 (2025).
24. Ritchie, P. D. L. et al. Shifts in national land use and food production in Great Britain after a climate tipping point. *Nat. Food* **1**, 76–83 (2020).
25. van Westen, R. M. & Baatsen, M. L. J. European temperature extremes under different AMOC scenarios in the Community Earth System Model. *Geophys. Res. Lett.* **52**, e2025GL114611 (2025).
26. Schaumann, F. & Alastrué de Asenjo, E. Weakening AMOC reduces ocean carbon uptake and increases the social cost of carbon. *Proc. Natl. Acad. Sci. USA.* **122**, e2419543122 (2025).
27. Callaghan, T. V. et al. Feedbacks and interactions: from the Arctic cryosphere to the climate system. *Ambio.* **40**, 75–86 (2011).
28. Yan, X. et al. Asynchronicity of deglacial permafrost thawing controlled by millennial-scale climate variability. *Nat. Commun.* **16**, 290 (2025).
29. Park, S.-W. et al. Continued permafrost ecosystem carbon loss under net-zero and negative emissions. *Sci. Adv.* **11**, eadn8819 (2025).
30. Wunderling, N. et al. Climate tipping point interactions and cascades: a review. *Earth Syst. Dyn.* **15**, 41–74 (2024).
31. MacDougall, A. H. et al. Is there warming in the pipeline? A multi-model analysis of the zero emissions commitment from CO_2. *Biogeosciences* **17**, 2987–3016 (2020).
32. Weijer, W., Cheng, W., Garuba, O. A., Hu, A. & Nadiga, B. T. CMIP6 models predict significant 21st century decline of the Atlantic Meridional Overturning Circulation. *Geophys. Res. Lett.* **47**, e2019GL086075 (2020).
33. Baker, J. A. et al. Overturning pathways control AMOC weakening in CMIP6 models. *Geophys. Res. Lett.* **50**, e2023GL103381 (2023).
34. Matthews, H. D., Gillett, N. P., Stott, P. A. & Zickfeld, K. The proportionality of global warming to cumulative carbon emissions. *Nature* **459**, 829–832 (2009).
35. MacDougall, A. H. The transient response to cumulative CO_2 emissions: a review. *Curr. Clim. Change Rep.* **2**, 39–47 (2016).
36. Mathison, C. et al. A rapid application emissions-to-impacts tool for scenario assessment: Probabilistic Regional Impacts from Model Patterns and Emissions (PRIME). *Geosci. Model Dev.* **18**, 1785–1808 (2025).
37. Arora, V. K. et al. Carbon-concentration and carbon-climate feedbacks in CMIP6 models and their comparison to CMIP5 models. *Biogeosciences* **17**, 4173–4222 (2020).
38. Sigmond, M., Fyfe, J. C., Saenko, O. A. & Swart, N. C. Ongoing AMOC and related sea-level and temperature changes after achieving the Paris targets. *Nat. Clim. Change* **10**, 672–677 (2020).
39. Ma, Q. et al. Revisiting climate impacts of an AMOC slowdown: dependence on freshwater locations in the North Atlantic. *Sci. Adv.* **10**, eadr3243 (2024).
40. Liu, W., Fedorov, A. V., Xie, S.-P. & Hu, S. Climate impacts of a weakened Atlantic Meridional Overturning Circulation in a warming climate. *Sci. Adv.* **6**, eaaz4876 (2020).
41. Schädel, C. et al. Earth system models must include permafrost carbon processes. *Nat. Clim. Change* **14**, 114–116 (2024).
42. MacDougall, A. H., Zickfeld, K., Knutti, R. & Matthews, H. D. Sensitivity of carbon budgets to permafrost carbon feedbacks and non-CO_2 forcings. *Environ. Res. Lett.* **10**, 125003 (2015).
43. Deutloff, J., Held, H. & Lenton, T. M. High probability of triggering climate tipping points under current policies modestly amplified by Amazon dieback and permafrost thaw. *Earth Syst. Dyn.* **16**, 565–583 (2025).
44. Nitzbon, J. et al. No respite from permafrost-thaw impacts in the absence of a global tipping point. *Nat. Clim. Change* **14**, 573–585 (2024).
45. Jackson, L. C., Chassignet, E. P., Danabasoglu, G., Treguier, A. & Zhang, R. Toward improving representation of the Atlantic Meridional Overturning Circulation in climate models. *Bull. Am. Meteorol. Soc.* **106**, E1032–E1036 (2025).
46. Terpstra, S. et al. Assessment of abrupt shifts in CMIP6 models using edge detection. *AGU Adv.* **6**, e2025AV001698 (2025).
47. Anthony, K. M. W. et al. A shift of thermokarst lakes from carbon sources to sinks during the Holocene epoch. *Nature* **511**, 452–456 (2014).
48. Brovkin, V. et al. Permafrost and freshwater systems in the Arctic as tipping elements of the climate system. *Surv. Geophys.* **46**, 303–326 (2025).

49. Drijfhout, S., Angevaare, J. R., Mecking, J., van Westen, R. M. & Rahmstorf, S. Shutdown of northern Atlantic overturning after 2100 following deep mixing collapse in CMIP6 projections. *Environ. Res. Lett.* **20**, 094062 (2025).
50. van Westen, R. M., Kliphuis, M. & Dijkstra, H. A. Physics-based early warning signal shows that AMOC is on tipping course. *Sci. Adv.* **10**, eadk1189 (2024).
51. Baker, J. A. et al. Continued Atlantic overturning circulation even under climate extremes. *Nature* **638**, 987–994 (2025).
52. Cui, M., Ji, D. & Chen, Y. Permafrost response and feedback under temperature stabilization and overshoot scenarios with different global warming levels. *Earth Syst. Dyn.* **16**, 1809–1831 (2025).
53. Ji, D., Cui, M., Chen, Y. & Dai, Y. Permafrost response in northern high latitude regions to 1.5°C warming and overshoot scenarios achieved via solar radiation modification. *J. Geophys. Res.* **130**, e2024JD041772 (2025).
54. Chen, Y., Moore, J. C. & Ji, D. Simulated responses and feedbacks of permafrost carbon under future emissions pathways and idealized solar geoengineering scenarios. *Environ. Res. Lett.* **19**, 024050 (2024).
55. Matthews, H. D., Zickfeld, K., Koch, A. & Luers, A. Accounting for the climate benefit of temporary carbon storage in nature. *Nat. Commun.* **14**, 5485 (2023).
56. Boselius, L., Duffey, A. & Irvine, P. J. Peak shaving with solar radiation modification would shorten global temperature overshoot. *Oxf. Open Clim. Change* **5**, kgaf013 (2025).
57. Quilcaille, Y., Gasser, T., Ciais, P. & Boucher, O. CMIP6 simulations with the compact Earth system model OSCAR v3.1. *Geosci. Model Dev.* **16**, 1129–1161 (2022).
58. Meredith, M. et al. *IPCC Special Report on the Ocean and Cryosphere in a Changing Climate*, Ch. Polar regions, 203–320 (Cambridge University Press, 2022).
59. Best, M. J. et al. The Joint UK Land Environment Simulator (JULES), model description—part 1: energy and water fluxes. *Geosci. Model Dev.* **4**, 677–699 (2011).
60. Clark, D. B. et al. The Joint UK Land Environment Simulator (JULES), model description—part 2: carbon fluxes and vegetation dynamics. *Geosci. Model Dev.* **4**, 701–722 (2011).
61. Chadburn, S. et al. An improved representation of physical permafrost dynamics in the JULES land-surface model. *Geosci. Model Dev.* **8**, 1493–1508 (2015).
62. Burke, E. J., Chadburn, S. E. & Ekici, A. A vertical representation of soil carbon in the JULES land surface scheme (vn4.3_permafrost) with a focus on permafrost regions. *Geosci. Model Dev.* **10**, 959–975 (2017).
63. Seland, y et al. Overview of the Norwegian Earth System Model (NorESM2) and key climate response of CMIP6 DECK, historical, and scenario simulations. *Geosci. Model Dev.* **13**, 6165–6200 (2020).
64. Tjiputra, J. F. et al. Ocean biogeochemistry in the Norwegian Earth System Model version 2 (NorESM2). *Geosci. Model Dev.* **13**, 2393–2431 (2020).
65. Danabasoglu, G. et al. The Community Earth System Model Version 2 (CESM2). *J. Adv. Model. Earth Syst.***12**, e2019MS001916 (2020).
66. Tjiputra, J. F. et al. Evaluation of the carbon cycle components in the Norwegian Earth System Model (NorESM). *Geosci. Model Dev.* **6**, 301–325 (2013).
67. Schwinger, J. et al. Evaluation of NorESM-OC (versions 1 and 1.2), the ocean carbon-cycle stand-alone configuration of the Norwegian Earth System Model (NorESM1). *Geosci. Model Dev.* **9**, 2589–2622 (2016).
68. Huntingford, C. & Cox, P. An analogue model to derive additional climate change scenarios from existing GCM simulations. *Clim. Dyn.* **16**, 575–586 (2000).
69. Zelazowski, P., Huntingford, C., Mercado, L. M. & Schaller, N. Climate pattern-scaling set for an ensemble of 22 GCMs—adding uncertainty to the IMOGEN version 2.0 impact system. *Geosci. Model Dev.* **11**, 541–560 (2018).
70. Riahi, K. et al. The shared socioeconomic pathways and their energy, land use, and greenhouse gas emissions implications: an overview. *Glob. Environ. Change* **42**, 153–168 (2017).
71. Wells, C. D., Jackson, L. S., Maycock, A. C. & Forster, P. M. Understanding pattern scaling errors across a range of emissions pathways. *Earth Syst. Dyn.* **14**, 817–834 (2023).
72. Huntingford, C. et al. IMOGEN: an intermediate complexity model to evaluate terrestrial impacts of a changing climate. *Geosci. Model Dev.* **3**, 679–687 (2010).
73. Mathison, C. et al. Description and evaluation of the JULES-ES setup for ISIMIP2b. *Geosci. Model Dev.* **16**, 4249–4264 (2023).
74. Andela, B. et al. ESMValTool *Zenodo*. https://doi.org/10.5281/zenodo.12654299 (2025).
75. Jones, C. D. et al. The Zero Emissions Commitment Model Intercomparison Project (ZECMIP) contribution to C4MIP: quantifying committed climate changes following zero carbon emissions. *Geosci. Model Dev.* **12**, 4375–4385 (2019).
76. Steinert, N. J. et al. Code and data availability information for "permafrost carbon release scales linearly with overshoot warming mediated by AMOC tipping" *Figshare* https://doi.org/10.6084/m9.figshare.30710540 (2026).

Author contributions

N.J.S., J.S. conceptualized the study. N.J.S., E.B., B.Z., T.G., and J.S. were responsible for data collection and curation. N.J.S. performed the analysis. N.J.S., J.S. prepared the manuscript with contributions from all co-authors. G.M., C.M., S.-W.P., and H.L. contributed to the writing of the manuscript.

Funding

N.J.S. has been funded by the Research Council of Norway through the project TRIFECTA (grant no. 334811) and by the European Commission through the project PROVIDE (grant 101003687). Further, N.J.S., J.S., and H.L. have been funded by the Research Council of Norway through the project IMPOSE (grant 294930). E.B. received funding from the European Union's Horizon 2020 research and innovation programme through the projects ESM2025 (grant 101003536) and OptimESM (grant 101081193), and the Met Office Hadley Centre Climate Programme funded by DSIT. B.Z., T.G., G.M., C.M., and S.-W.P. declare no relevant funding. The work reflects only the authors' view; the European Commission and their executive agency are not responsible for any use that may be made of the information the work contains.

Competing interests

The authors declare no competing interests.

Additional information

Supplementary information The online version contains Supplementary material available at https://doi.org/10.1038/s41467-026-73612-0.

Correspondence and requests for materials should be addressed to Norman Julius Steinert.

Peer review information *Nature Communications* thanks Xu Zhang, who co-reviewed with Xinwei Yan and the other anonymous reviewer(s) for their contribution to the peer review of this work. A peer review file is available.

https://doi.org/10.1038/s41467-026-73612-0